Quantitative combined multiscale structural and minero-chemical analysis to unravel the tectono-metamorphic evolution of cordierite-migmatite gneiss from the Valpelline Unit (Dent-Blanche Nappe, Western Italian Alps, Valle d'Aosta)

Fabiola Caso[1]

[1] Dipartimento di Scienze della Terra "A. Desio", Università degli Studi di Milano, Via Mangiagalli 34, 20133, Milan, Italy.

FC, 0000-0002-1136-2811.

Rend. Online Soc. Geol. It., Vol. 60 (2023), pp. 13-21, 4 figs., https://doi.org/10.3301/ROL.2023.20

Article

Corresponding author e-mail: fabiola.caso@unimi.it

Citation: Caso F. (2023) - Quantitative combined multiscale structural and minero-chemical analysis to unravel the tectono-metamorphic evolution of cordierite-migmatite gneiss from the Valpelline Unit (Dent-Blanche Nappe, Western Italian Alps, Valle d'Aosta). Rend. Online Soc. Geol. It., 60, XX-XX, https://doi.org/10.3301/ROL.2023.20 .

Guest Editor: Alessandro Petroccia

Submitted: 25 November 2022

Accepted: 31 January 2023

Published online: 18 April 2023

ABSTRACT

Among the Valpelline Unit migmatites, the cordierite-bearing ones represent the most fascinating type, but little is known about their *P-T* evolution. Since the complete understanding of these rocks results from the interplay of petrological and multiscale structural investigations, a multidisciplinary approach that combines quantitative microstructural and minero-chemical data, discriminating different generations of superimposed foliations and stages is provided. Two main deformational stages have been defined at the meso- and microscale: the first (D_1) is a solid-state deformation developing a foliation (S_1) preserved as isoclinal folds; the second (D_2) is related to the development of the main foliation (S_2), associated with cordierite and garnet growth, and melt production. The regional S_2 wraps cordierite, garnet and melt aggregates. Temperatures for the cordierite-growing stage, obtained by combining biotite calibrated maps and Ti-in-biotite thermometer, range between ~700 and 780 °C.

KEY-WORDS: high-temperature metamorphism, mineral grain orientations, X-ray chemical mapping, cordierite, migmatite.

INTRODUCTION

Cordierite-bearing migmatites widely occur in cratons and orogenic belts worldwide (e.g., Higher-Himalayan Crystalline; Groppo et al., 2013; Ivrea-Verbano Zone in the Western Alps; Redler et al., 2012). Much of the published work on cordierite-bearing migmatites has concentrated mainly on the petrological processes that have changed the sedimentary, igneous or metamorphic protoliths into migmatites, giving less relevance to the structural relationships occurring between the cordierite-growth and melt-present deformation. Unraveling the evolution of this kind of rock could be tricky due to the presence of melt produced during the deformation which makes several superimposed geometric patterns resulting in a complex structural architecture at all scales (Sawyer, 2000; Sawyer, 2008; Kreigsman & Alvarez-Valero, 2010; Yakymchuk, 2020 and references therein). In the Valpelline Unit, previous authors described cordierite-bearing migmatites (Gardien et al., 1994), but without clearly putting them in a framework of a detailed multiscale structural evolution. Geological mapping and outcrop-scale studies for the description of geometrical overprinting relationships are fundamental starting tools in structural geology (e.g., Spalla et al., 2005; Caso et al., 2021; Petroccia et al., 2020, 2022), but they need to be integrated with quantitative microstructural and chemical data to be fully understood (Spalla & Zucali, 2004; Fazio et al., 2009; Corti et al., 2019; Roda et al., 2021; Zucali et al., 2021). Quantitative parameters such as grain-size distribution, mineral shape factors and orientations, measured using ArcGis "ready-to-run" toolboxes, on the main rock-forming mineral phases, could be combined with quantitative minero-chemical data (i.e., calibrated X-ray maps and point mineral analyses). This approach aims to discriminate different generations of fabric elements (i.e., superimposed foliations) and their respective marking mineral assemblages. The present work shows the application of these methods on one specimen of cordierite-

migmatite gneiss from the Valpelline Unit (Western Italian Alps). This unit belongs to the Dent-Blanche Nappe (Manzotti et al., 2014) of the Austroalpine Domain and represents an excellent example of partially melted rocks from the lower continental crust, characterized by a high-temperature/low-pressure (H*T*-L*P*) metamorphic imprint, of pre-Alpine age (Diehl et al., 1952; Nicot, 1977; Gardien et al., 1994; Zucali et al., 2011; Pesenti et al., 2012; Manzotti & Zucali, 2013; Kunz et al., 2018). Cordierite occurring in migmatites from the Valpelline Unit has been described to be related to a stage of migmatization after the development of the main pre-Alpine regional foliation (Gardien et al., 1994). In this regard, the applied multiscale structural approach coupled with mineral chemistry allows the reconstruction of the Valpelline Unit tectono-metamorphic evolution and inferring the relative timing of cordierite and garnet growth in migmatites. In particular, the Micro-Fabric Analyzer ArcGIS toolbox (Visalli et al., 2021) has been applied to a high-resolution thin section optical scan coupled with the Quantitative X-Ray Maps Analyzer tool (Q-XRMA; Ortolano et al., 2018) to derive quantitative textural and compositional data to distinguish different foliations at the microscale basing on long axis grain orientations. Moreover, wavelength-dispersive spectrometer (WDS) quantitative mineral point analyses have been used to calibrate maps showing the element content within some mineral phases (i.e., biotite and garnet) in order to check the presence of chemical zoning and use it as a constrain for the distinction of the stages related to the migmatization in the Valpelline Unit, and preliminarily infer its thermal conditions.

GEOLOGICAL SETTING

The Valpelline Unit (Western Italian Alps) belongs to the Dent-Blanche Nappe (Manzotti et al., 2014), which consists in a continental klippe of the Austroalpine domain that structurally covers the metaophiolitic units of the Piedmont-Ligurian Ocean (Basic and Ultrabasic in Fig. 1a). The Dent-Blanche Nappe is classically divided into the Dent-Blanche s.s. to the northwest and the Mont-Mary Nappe to the southwest separated by the Rosain-Cignana Shear Zone (Manzotti et al., 2014). The Dent-Blanche s.s. is made of a Paleozoic basement corresponding to the Arolla and the Valpelline units (Diehl et al., 1952; Manzotti & Zucali, 2013; Manzotti et al., 2014). This continental nappe recorded both pre-Alpine and Alpine metamorphism: the former is related to Variscan and post-Variscan high-temperature regimes and is mainly preserved in the Valpelline Unit (Gardien et al., 1994; Manzotti & Zucali, 2013), and the latter is in blueschist/greenschist-facies and is pervasive in the Arolla Unit. The Valpelline Unit consists of high-grade gneiss affected by partial melting with associated pegmatitic dikes, lenses of garnet-clinopyroxene amphibolites, basic granulites and marbles (Fig. 1b; Diehl et al., 1952; Nicot, 1977; Gardien et al., 1994; Manzotti & Zucali, 2013). Regarding the pre-Alpine history, the first recognized tectono-metamorphic event (MZ1 in figure 1c; T = 700 ± 50°C and P = 5.7 ± 1 kbar; Manzotti & Zucali, 2013) is marked by a relict foliation (S_{pre2} in Manzotti & Zucali, 2013) preserved within metabasite and marble boudins enclosed within metapelites. Gardien et al. (1994) also defined a relict stage (G1; Fig. 1c), preserved only in garnet cores with kyanite inclusions (T = 700–800°C and P = 9–10 kbar). The penetrative stage, related to melt production and S_2 foliation development (G2a, G2b and MZ2 in figure 1c) occurs at T = 750–800°C and P = 5–7 kbar. During the third stage (T = 800 ± 30°C and P = 6 ± 0.7 kbar; Manzotti & Zucali, 2013), the S_2 is isoclinally folded, leading to the development of an S_3 axial plane foliation, marked by Bt + Sil both at the meso- and microscale. Moreover, Gardien et al. (1994) recognized a further migmatitic stage (G3; Fig. 1c) associated with the cordierite growth, estimated at T = 650–700 °C and P = ~3.5–4.5 kbar. S_2 and S_3 are parallel to the lithological boundaries, strike NE-SW and dip at high-angle (Manzotti & Zucali, 2013). The D_2 stage has been dated to Permian (U–Pb geochronology; Zucali et al., 2011; Pesenti et al., 2012; Kunz et al., 2018). The Alpine imprint (T = 430 ± 30°C and P = 3–5 kbar; Gardien et al., 1994; Manzotti & Zucali, 2013; stages G4 and MZ4 in figure 1c) is weak and localized only along some decametric to hectometer-wide shear zones. The Valpelline Unit is compared to other Adria-derived crustal portions, i.e., the Ivrea-Verbano Zone and Seconda Zona Diorito-Kinzigitica (Fig. 1a) due to their lithological similarities and comparable high-temperature pre-Alpine metamorphic conditions and age (e.g., Redler et al., 2012; Kunz et al., 2018). Despite these similarities, a thorough understanding of the complex tectono-metamorphic evolution related to the migmatization is needed to constrain the role of the Valpelline Unit in the geodynamic framework of the Permian lithospheric extension, together with the Ivrea-Verbano Zone and Seconda Zona Diorito-Kinzigitica equivalents.

APPROACH AND METHODOLOGIES

Field observations and measurements of the main fabric elements (i.e., foliations and fold axes) of the cordierite-bearing outcrop localities have been carried out, coupled with the determination of their marking minerals and rock sampling. A cordierite-migmatite gneiss (sample 33SC; see Fig. 1b for its location) from the Valpelline Unit (west of Vessonaz stream; WGS84 coordinates: N 45°50'31" E 7°25'37") was first analyzed at the optical microscope to understand the relationship between the mesoscopic fabric elements and their marking mineral phases, following the guidelines of Passchier & Trouw (2005) and Spalla et al. (2005). Mineral abbreviations used in the text are after Whitney & Evans (2010), except for Wm (i.e., white mica). Chemical analyses on the mineral phases making up the chosen sample (i.e., sillimanite, biotite, garnet, cordierite, white mica, plagioclase, ilmenite, chlorite and rutile) were carried out with the Electron Microprobe Analyser (EMPA) Jeol 8200 Superprobe (WDS) at the Dipartimento di Scienze della Terra "A. Desio" – Università degli Studi di Milano to derive quantitative mineral point chemical analyses and X-ray chemical maps of major (Si, Ti, Al, Fe, Mn, Mg, Ca, Na, K) and minor elements (Cr). Fe, Mg, Ti, Ca and Na maps were acquired using five WDS detectors, Si, Al, Mn, Cr and K using energy-dispersive spectrometer (EDS) detector. For mineral analyses an accelerating voltage of 15 KeV and 50 nA of

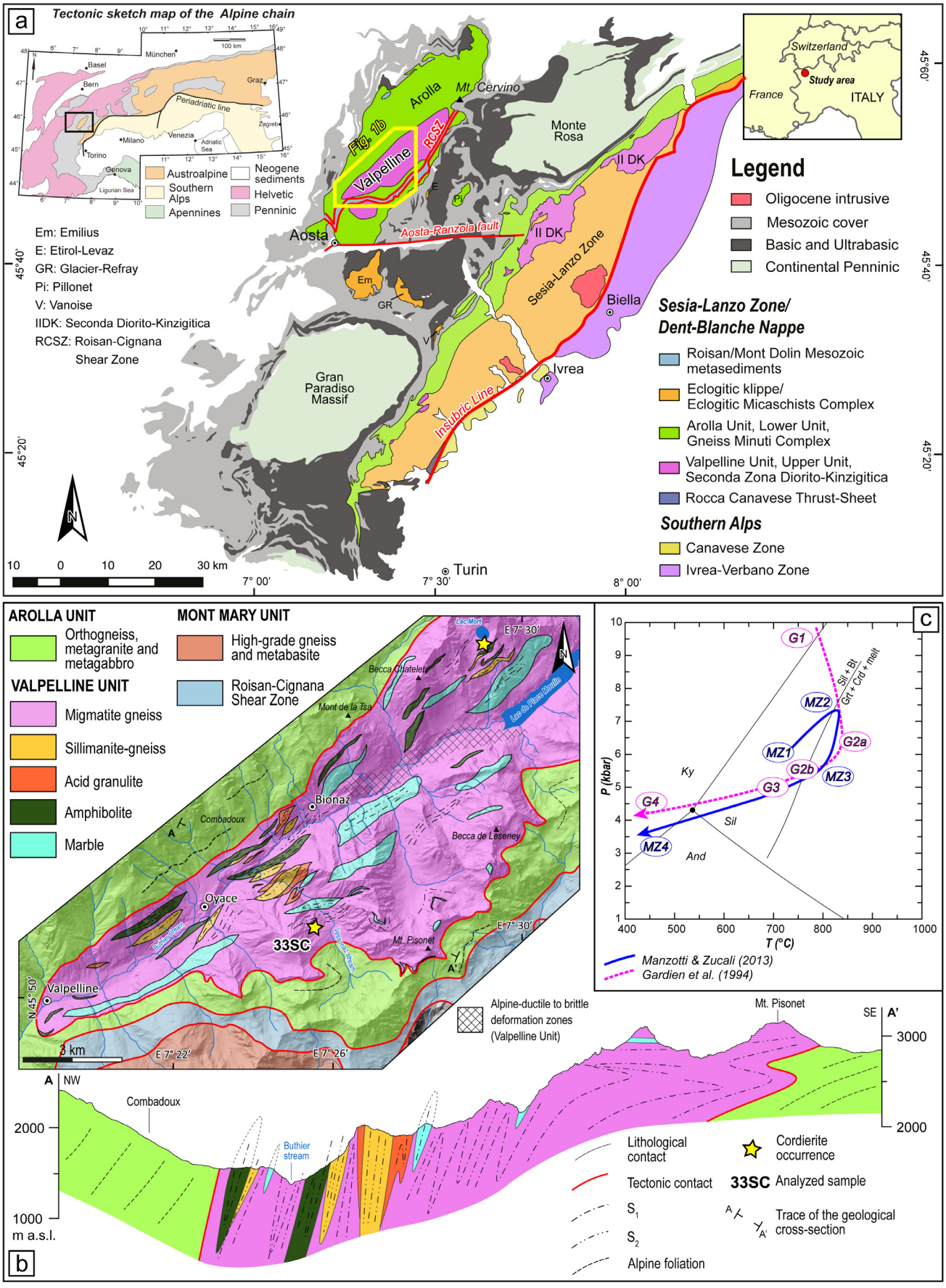

Fig. 1 - a) tectonic sketch map of the Alps (top left side) and tectonic sketch map of the Western Alps, highlighting Adria-derived units (modified after Roda et al., 2021); b) schematic geological map and cross-section (A-A') of part of the study area; c) *P–T* conditions of the Valpelline Unit for different tectono-metamorphic stages estimated by Gardien et al. (1994) and Manzotti & Zucali (2013). Ky, And and Sil stability fields have been calculated after Holland & Powell (2011) and the Crd-in reaction is after White et al. (2014).

beam current was used, while for X-ray mapping the beam current was of 100 nA, with a dwell time of 55 ms and a resolution 1024 * 600 pixels (35 µm of step size). The Micro-Fabric Analyzer ArcGis toolbox (MFA; Visalli et al., 2021) was used to obtain the contouring of the mineral grains and measure their shape parameters (see Visalli et al., 2021 Appendix A for the explanation of the calculated values). This tool allows the reconstruction of mineral grain-polygon maps by combining data from a high-resolution optical thin section scan (grain boundaries and polygon vector maps through the Grain-Size Detector toolbox; GSD, Visalli et al., 2021) and mineral classification grains map obtained from X-ray maps processing through the Q-XRMA tool (Ortolano et al., 2018). As a result, each grain (containing its shape parameters) will be labeled with a mineral phase name. The thin section scan was acquired under crossed polarized light by using an Epson V750 dual-lens system scanner at 24 bit-depth and 4800 dpi of resolution corresponding to a pixel size of ~5.29 µm, which according to Visalli et al. (2021), represents the best compromise among high-quality imagining, relatively fast image-processing time and reasonable hard drive space storage. EMPA minero-chemical data have been used as internal standards in XMapTools v.4 (Lanari et al., 2014) to make element-calibrated maps of different mineralogical phases (i.e., garnet and biotite). Each pixel of these calibrated maps has a specific quantitative value related to a chemical element a.p.f.u. content in each mineral phase. Moreover, temperatures using the Ti-in-biotite thermometer (Henry et al., 2005), through the add-on included in XMapTools v.4, were obtained from each classified pixel of the Ti a.p.f.u. map calibrated using the EMPA quantitative mineral analyses on biotite.

RESULTS

Petrographical and structural analysis

Meso- and microstructural analysis of cordierite-migmatites led to the definition of two deformation stages: (i) D_1 and (ii) D_2. The D_1 stage is preserved as the S_1 foliation marked by sillimanite + biotite-rich pluri-mm-thick films alternating with pluri-mm- to pluri-cm- quartzo-feldspathic lithons. At the mesoscale, the S_1 is preserved as folded layers (Fig. 2a) or disrupted fold hinges. At the microscale, the S_1 is marked by the Shape Preferred Orientation (SPO) of sillimanite and minor biotite (Sil I; Figs. 2b, c) within mm-spaced microlithons. Between D_1 and D_2, the growth of pluri-cm cordierite (Fig. 2a) and garnet porphyroblasts occurs. D_2 deformation folds (Fig. 2a) and locally transposes the previous S_1 foliation developing the S_2 which is the most penetrative fabric in sillimanite-rich migmatites (Fig. 2b), and mainly dips toward the SE and NW with sub-vertical dip angles (see foliation traces in the geological map and cross-section in Fig. 1b). The S_2 is marked by the SPO of sillimanite and biotite lamellae (i.e., Sil II and Bt II in Figs. 2b, c, d, e) and wraps around cordierite and garnet porphyroblasts. Garnet porphyroblasts include rounded biotite (Bt I), sillimanite (Sil I) and quartz inclusions, likely related to the D_1 stage. These inclusions highlight an internal S_1 foliation, discordant in the core and in continuity with the external S_2 in the rim (Fig. 2e), thus growing from inter- to syn-kinematic (Passchier & Trouw, 2005) with respect to the S_2 foliation. Biotite and sillimanite wrap around cordierite porphyroblasts (Fig. 2d) or locally grow static over it (Fig. 2f). Fine-grained aggregates of white mica locally overgrow cordierite and plagioclase.

Quantitative microstructural analysis: the Micro-Fabric Analyzer method

A thin section XPL scan was used as input in GSD included in the MFA toolbox (Fig. 3a); then, the GSD tool outputs a polygonal map (i.e., GIS layer) of the grains, with no phase discrimination. Subsequently, chemical X-ray maps (Fig. 3b) were used to obtain a mineral classification map (Q-XRMA) without grain boundaries. The Q-XRMA tools also provided the modal percentages (%) of the mineral phases (cake diagram in Fig. 3c). The Mineral-Grain-Size detector tool (Min-GSD), included in the MFA toolbox, combines GSD and Q-XRMA, and outputs a vectorial grain polygon map whose grains are labeled with a mineral phase attribute (Fig. 3c). As a result, rock-forming mineral grains have been distinguished: 15,058 sillimanite grains, 4,049 biotite grains, 1,277 garnet grains, 757 white mica grains, 432 cordierite grains, 397 plagioclase grains, 384 ilmenite grains, 311 quartz grains, 127 chlorite grains and 11 rutile grains. Grain-orientation data have been calculated from each mineralogical phase and used to discriminate between S_1 and S_2 fabrics. In particular, the long axis orientation angles (0°–180°) measured clockwise from a reference vertical axis have been plotted (Fig. 3d) for sillimanite, biotite, ilmenite and garnet. In particular, sillimanite, biotite and ilmenite have been chosen for the quantitative microstructural analysis since their habitus is suitable for highlighting oriented fabrics as foliations. Garnet has been also reported to check whether a slight orientation of these grains occurs. Sillimanite long axis orientations are homogeneous, with the main cluster at ~90°, highlighting the S_2 foliation (Figs. 3d, e). The other orientations (i.e., ~60 or ~120°) mark the S_1 crenulations within microlithons (Figs. 3d, e). Most of the biotite long axis orientations have values of about ~90°, with two minor clusters at ~ 60° and ~120°. Relatively few grains have 0° or 180° of long axis orientation. In this case, the first most frequent cluster highlights the S_2 main foliation, while the other minor ones refer to S_1 crenulation within microlithon, or Bt I grains included within garnet porphyroblasts (see the red square in Fig. 3f). Ilmenite grains show different clusters of the long axis orientation. However, the most frequent is the one at ~90° as for sillimanite and biotite (Fig. 3d) again marking the S_2 foliation. Garnet orientation values have also been plotted, but they appear more scattered, with a weak cluster again at ~90°. The long axis orientation maps exported from ArcGIS for sillimanite (Fig. 3e) and biotite (Fig. 3f) grains highlight the principal foliation S_2. Most of the red and blue grains correspond to minerals included within garnet porphyroblasts (i.e., Bt I), in strain shadows (Bt II) or marking the microfolded S_1 foliation (Sil I and Bt I).

Microchemical characterization and temperature estimations

Among the analyzed mineral phases, only garnet and biotite show a clear chemical zoning, visible both from the mineral point EMPA analyses and the calibrated X-ray maps; thus this analysis

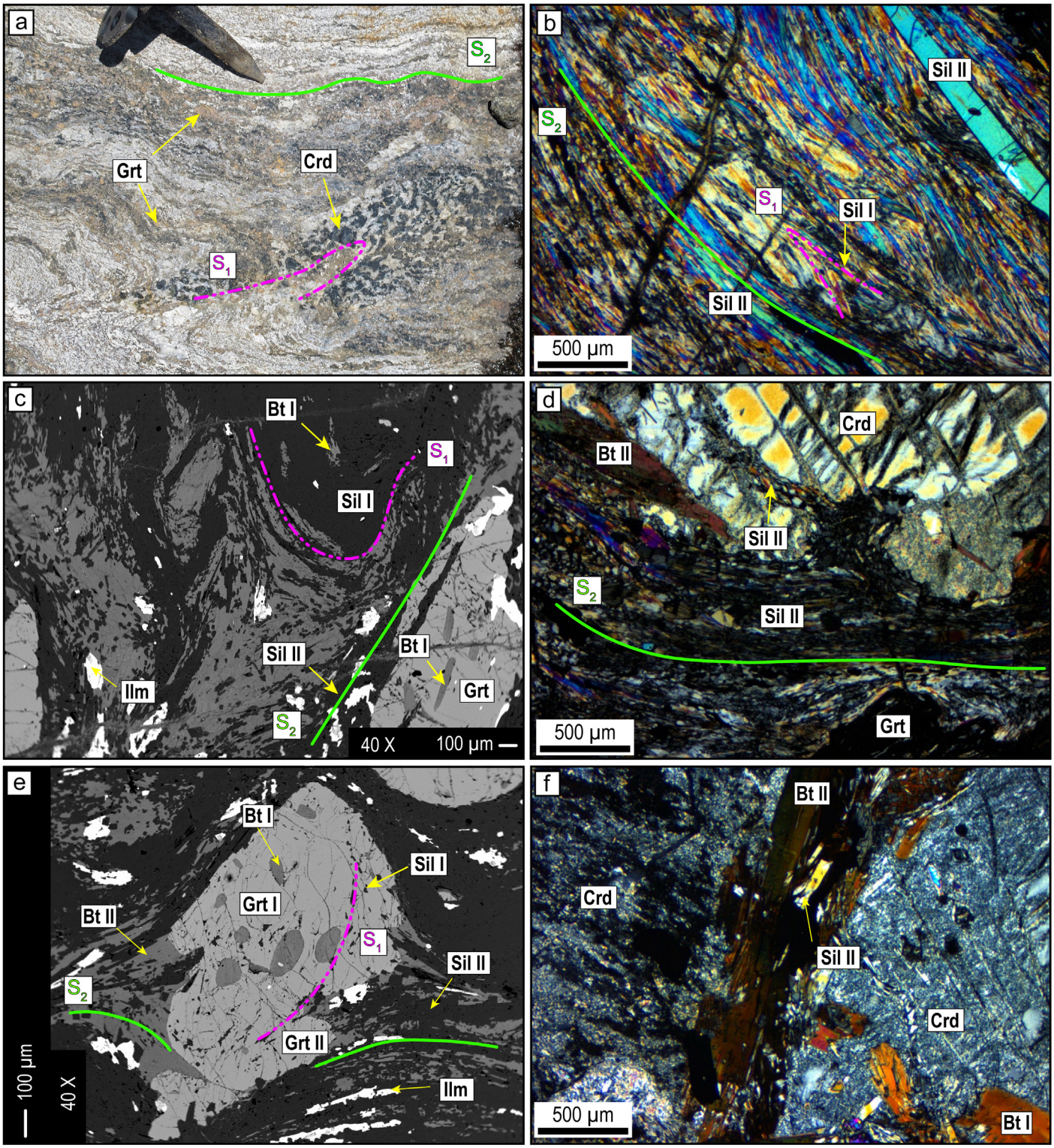

Fig. 2 - a) outcrop view of isoclinally folded leucosome (S_1 foliation) with gray centimetric cordierite porphyroblasts; the S_2 foliation in fine-grained portions is made by the transposition of the S_1 one; b) S_2 foliation marked by Sil II SPO and CPO (Crystallographic Preferred Orientation) and folded Sil I within microlithons (XPL: crossed-polarized light); c) S_1 folded foliation made by deformed Sil I and Bt I (BSE; back-scattered electron); d) microscale detail of cordierite and garnet wrapped by the Sil II-rich foliation S_2 (XPL); e) inter- to syn-kinematic garnet porphyroblast (Grt I and Grt II respectively) wrapped by S_2 foliation, showing an internal foliation S_1 discordant and locally concordant with respect to the S_2 (BSE); f) detail of cordierite porphyroblast overgrown by Sil II and Bt II (XPL).

focuses only on these two phases. Garnet calibrated maps have been obtained using 40 EMPA spot analyses homogenously distributed within the sample. *XPrp* (pyrope), *XAlm* (almandine) and *XGrs* (grossular) maps show a slight chemical zoning, highlighting a garnet core and garnet rim (Figs. 4a, b). The *XPrp* (Mg/Mg+Fe+Ca+Mn) decreases from the core (~0.24–0.29) to the rim (~0.22–0.24) of the garnet, while the *XAlm* (Fe/Fe+Mg+Ca+Mn) slightly increases from the core (~0.68–0.72;

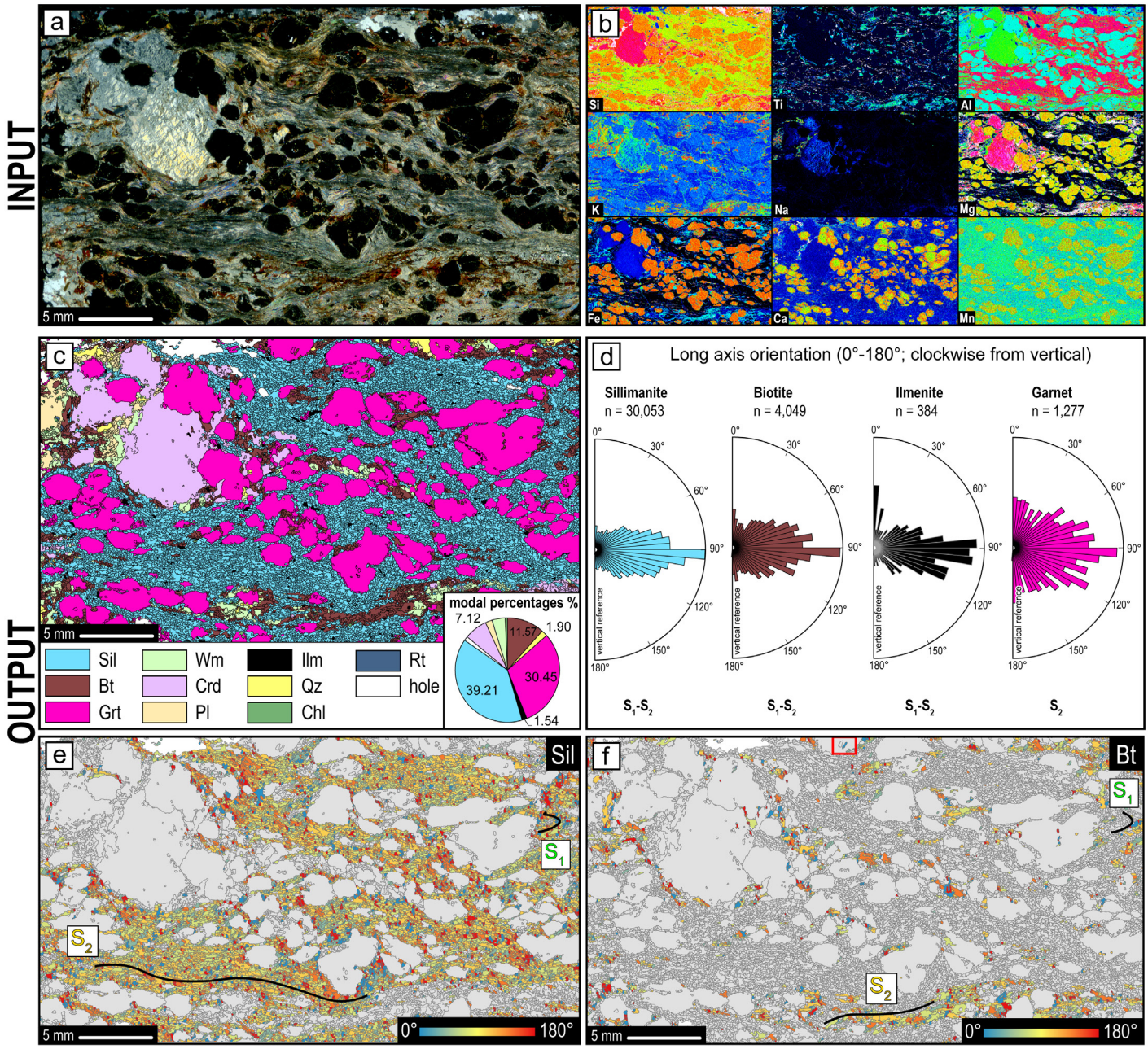

Fig. 3 - Inputs and outputs of the Micro-Fabric Analyzer procedure. a) Thin section high-resolution scan in XPL of the analyzed sample used as input in the GSD tool; b) WDS and EDS chemical X-ray maps used in the Q-XRMA tool to obtain the mineral maps and the modal percentages. c) Mineral grains classified map output obtained from the Min-GSD; d) long axis grain orientation circular distribution diagram of S_1 and S_2 foliations for different mineralogical phases; e) long axis orientation map of sillimanite grains; f) long axis orientation map of biotite grains; the red square highlights an example of biotite included in garnet with long axis orientation different respect to those marking the S_2.

Fig. 4a) to the rim (~0.72–0.75; Fig. 4a). *XGrs* (Ca/Ca+Fe+Mg+Mn) also increases from the core (~0.019–0.022; Fig. 4b) to the rim (~0.022–0.029; Fig. 4b). The obtained biotite calibrated map (60 EMPA spot analyses used) for the Ti a.p.f.u. (atoms per formula unit) content shows a variation between 0.25 and 0.7 a.p.f.u. (Figs. 4c, d). The Ti content is higher in biotite included in garnet, deformed biotite that marks the S_1 relict foliation and in the core of some biotite lamellae along the S_2 (Fig. 4c). The Ti concentration is lower in correspondence of some biotite growing after cordierite, and the rim of biotite along the main foliation S_2. *XMg* (Mg/Mg+Fe) shows only a slight variation between 0.52 and 0.64 (Fig. 4d). From each pixel data, the tool calculates temperatures (°C) using the Ti-in-biotite geothermometer, calibration of Henry et al. (2005). The obtained temperature map and the histogram highlight how most of *T* °C is comprised between ~700 and ~780 °C (Figs. 4d, e, f), with a mean temperature of 724 °C ± 24 (Fig. 4f).

DISCUSSIONS AND CONCLUSIONS

The combination of quantitative meso- and microstructural analysis with minero-chemical results on the cordierite-migmatite gneiss of the Valpelline Unit allowed to define two tectono-

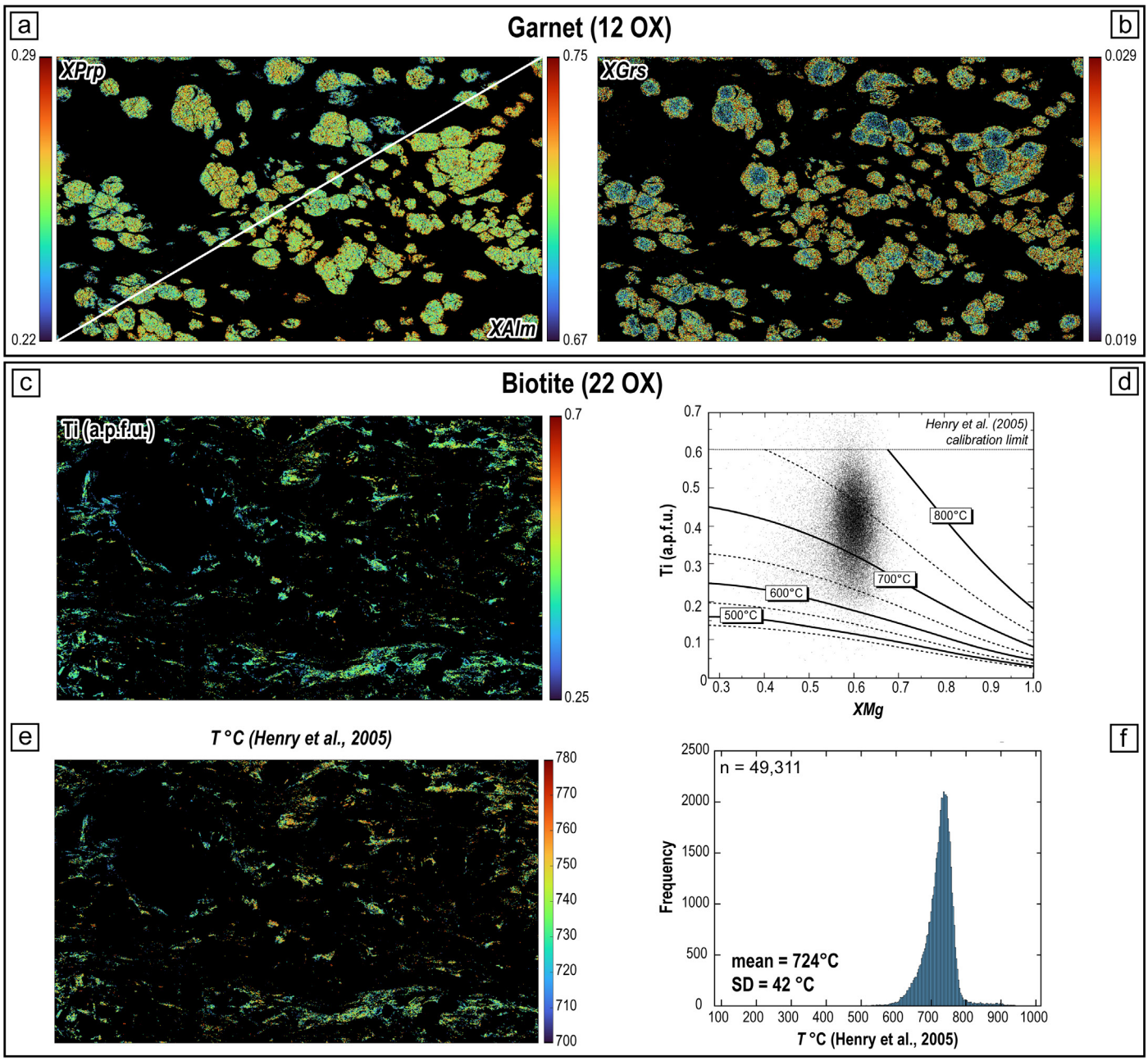

Fig. 4 - XMapTools outputs: a) XPrp and XAlm map in garnet; b) XGrs map in garnet; c) Ti a.p.f.u. content calibrated map in biotite; d) XMg vs Ti (a.p.f.u.) plotted data derived from the calibrated pixels. Isotherms for *T* (°C) are after Henry et al. (2005); e) *T* (°C) map obtained using the Henry et al. (2005) calibration of the Ti-in-biotite geothermometer; f) frequency histogram showing the obtained temperatures from each pixel of the calibrated map.

metamorphic stages, D_1 and D_2 at the meso- and microscale. Mesoscale observations and petrographical analyses have been integrated with quantitative microstructural data obtained through the MFA method (Visalli et al., 2021) and quantitative chemical ones derived from calibrated maps through XMapTools (Lanari et al., 2014). Considering mineral grains data obtained from the MFA, the D_1-related microstructures (i.e., the relicts of the S_1 foliation) are highlighted by the scattered long axis orientations of biotite and sillimanite grains, and minor clusters at 60° or 120° (Fig. 3d), corresponding to microfolds hinges, or inclusions in cordierite and garnet porphyroblasts (Figs. 4e, f). This stage is also clearly distinct from a mineral composition and chemical point of view; it corresponds to high Ti a.p.f.u. biotite that occurs as rounded inclusions within garnet or pre-kinematic biotite to the S_2. Stage D_2 is supported by the cluster of long axis orientations of sillimanite, biotite, and ilmenite (Fig. 3d) that lay almost parallel to the S_2 main foliation (Figs. 4e, f). The Prp-rich/Alm-poor/Grs-poor garnet core (Fig. 4a) is inter-kinematic with respect to the S_2 foliation (Grt I in Fig. 2c), the Prp-poor/Alm-rich/Grs-rich garnet rim grows syn-kinematically to the S_2 (Grt II in Fig. 2c). Therefore, garnet growth occurs between D_1 and D_2 stages and continues also during the S_2 foliation development. Garnet long axis orientations are strongly scattered (Fig. 3d) because of their high isotropy (see Fig. 3a) and because most of the grains are pre-kinematic (inter-kinematic) with respect to S_2 foliation (Fig. 2c).

This work shows that cordierite grows before the development of the main S_2 foliation (i.e., the D_2 stage; Figs. 2a, d). Previous authors, on the contrary, have outlined that cordierite developed in a second migmatitic stage after the main regional foliation development (i.e., stage G3 of Gardien et al. 1994; Fig. 1c). Since cordierite is, along with garnet, wrapped by the S_2 foliation (i.e., the S_3 of Manzotti & Zucali, 2013) or locally substituted by biotite and sillimanite, both cordierite and garnet are interpreted as peritectic minerals that grow in the presence of melt resulting from the incongruent melting of biotite. Moreover, the analyzed sample shows a relatively large modal abundance of sillimanite (~40 % vol; Fig. 3c), mostly marking the main S_2 foliation. Sillimanite (and minor biotite) foliation could be produced in two ways: (i) by the destabilization of white mica according to the reaction Ms + Qz = Sil + Kfs + melt or (ii) during retrogression in the presence of melt by crossing the reaction Grt + Crd + melt = Bt + Sil (Kreigsman & Alvarez-Valero, 2010; White et al., 2014; reaction curve in Fig. 1c). In the analyzed sample most of the sillimanite is present along the main foliation that wraps the peritectic mineral (Figs. 2d, e); thus it is interpreted as a back-reaction product in the presence of melt (Kreigsman & Alvarez-Valero, 2010).

Temperatures estimated through the Ti-in-biotite thermometer (Henry et al., 2005) fall between ~700 and 780 °C (Figs. 4d, e, f). The higher temperatures correspond to Bt I included in garnets, deformed Bt I that marks the S_1 relict foliation and in the core of several biotite lamellae along the S_2 (Bt II; Fig. 4e). The obtained *T* °C are consistent with the literature (e.g., Gardien et al., 1994; Manzotti & Zucali, 2013) on migmatites and biotite-sillimanite gneiss of the Valpelline Unit by using various geothermometers (e.g., garnet-biotite exchange; Ti-in-biotite). Nevertheless, thermodynamic modeling is needed to better constrain the *P*–*T* conditions of each tectono-metamorphic stage.

In conclusion, the described quantitative multiscale multidisciplinary allows defining two main deformational stages (D_1 and D_2) defined by two superimposed foliations (S_1 and S_2) recognized at the meso- and microscale. Garnet and cordierite grow between the D_1 and D_2 stages together with melt production and are wrapped by the S_2 foliation made by SPO of sillimanite and biotite, as quantitatively demonstrated through the MFA tool. The applied innovative approach can be extended to the entire Valpelline Unit, analyzing more samples and applicating more geothermometers and geobarometers (e.g., Zr-in-rutile thermometer; Thomkins et al., 2007), coupled with U–Pb geochronology on rutile, zircon or monazite (e.g., Pesenti et al., 2012), to obtain a fully constrained *P*–*T*–D–*t* history of the Valpelline Unit.

ACKNOWLEDGMENTS

I would like to thank my supervisor Prof. Michele Zucali for supporting and supervising my PhD research activities and ideas. Many thanks also to Dr. Roberto Visalli for the help in the use of Micro-Fabric Analyzer and Q-XRMA tools. Andrea Risplendente is also thanked for his assistance during EMPA analytical sessions. I am grateful to an anonymous reviewer and Prof. Eugenio Fazio for their useful comments and suggestions that helped to improve the quality of the manuscript. This work is funded by "ProDe – Progetto d'Eccellenza – Le geoscienze per la società: risorse e loro evoluzione – 2018-2022" and "PSR2020_MRODA".

REFERENCES

Caso F., Nerone S., Petroccia A. & Bonasera M. (2021) - Geology of the southern Gran Paradiso Massif and Lower Piedmont Zone contact area (middle Ala Valley, Western Alps, Italy). J. Maps, 17(2), 237-246, https://doi.org/10.1080/17445647.2021.1911869.

Corti L., Zucali M., Visalli R., Mancini L. & Mohammad S. (2019) - Integrating X-ray computed tomography with chemical imaging to quantify mineral re-crystallization from granulite to eclogite metamorphism in the Western Italian Alps (Sesia-Lanzo Zone). Front. Earth. Sci., 7, 327, https://doi.org/10.3389/feart .2019.00327.

Diehl E.A., Masson R. & Stutz A.H. (1952) - Contributo alla conoscenza del ricoprimento della Dent Blanche. Memorie degli Istituti di Geologia e Mineralogia dell'Università di Padova, 17, 1-52.

Fazio E., Cirrincione R. & Pezzino A. (2009) - Garnet crystal growth in sheared metapelites (southern Calabria-Italy): Relationships between isolated porphyroblasts and coalescing euhedral crystals. Periodico di Mineralogia, 78(1).

Gardien V., Reusser E. & Marquer D. (1994) - Pre-Alpine metamorphic evolution of the gneisses from the Valpelline Series (Western Alps, Italy). Schweizerische Mineralogische und Petrographische Mitteilungen, 74, 489-502.

Groppo C., Rolfo F. & Mosca P. (2013) - The cordierite–bearing anatectic rocks of the higher Himalayan crystallines (eastern Nepal): low–pressure anatexis, melt productivity, melt loss and the preservation of cordierite. J. Metam. Geol., 31(2), 187-204, https://doi.org/10.1111/jmg.12014.

Henry B., Guidotti C.V. & Thomson J.A. (2005) - The Ti-saturation surface for low-to-medium pressure metapelitic biotite: implications for geothermometry and Ti-substitution mechanisms. Am. Mineral., 90, 316-28, https://doi.org/10.2138/am.2005.1498.

Holland T.J.B. & Powell R. (2011) - An improved and extended internally consistent thermodynamic dataset for phases of petrological interest, involving a new equation of state for solids. J. Metam. Geol., 29(3), 333-383, https://doi.org/10.1111/j.1525-1314.2010.00923.x.

Kriegsman L.M. & Alvarez-Valero A.M. (2010) - Meltproducing versus melt-consuming reactions in pelitic xenoliths and migmatites. Lithos, 116, 310-320, https://doi.org/10.1016/j.lithos.2009.09.001.

Kunz B.E., Manzotti P., von Niederhäusern B., Engi M., Darling J.R., Giuntoli F. & Lanari P. (2018) - Permian high-temperature metamorphism in the Western Alps (NW Italy). Int. J. Earth Sci., 107, 203-229, https://doi.org/10.1007/s00531-017-1485-6.

Lanari P., Vidal O., De Andrade V., Dubacq B., Lewin E., Grosch E.G. & Schwartz S. (2014) - XMapTools: a MATLAB© -based program for electron microprobe X-ray image processing and geothermobarometry. Comp. Geosci. 62, 227-240, https://doi.org/10.1016/j.cageo.2013.08.010.

Manzotti P. & Zucali M. (2013) - The pre-Alpine tectonic history of the Austroalpine continental basement in the Valpelline unit (Western Italian Alps). Geol. Mag., 150, 153-172, https://doi.org/10.1017/S0016756812000441.

Manzotti P., Ballèvre M., Zucali M., Robyr M. & Engi M. (2014) - The tectonometamorphic evolution of the Sesia–Dent Blanche nappes (internal Western Alps): review and synthesis. Swiss J. Geosci., 107(2), 309-336, https://doi.org/10.1007/s00015-014-0172-x.

Nicot E. (1977) - Les roches meso et catazonales de la Valpelline (nappe de la Dent Blanche, Alpes italiennes) (Doctoral dissertation, éditeur inconnu).

Ortolano G., Visalli R., Gaston G. & Cirrincione R. (2018) - Quantitative X-ray Map Analyser (Q-XRMA): A new GIS-based statistical approach to Mineral Image Analysis. Comp. Geosci., 115, 56-65, https://doi.org/10.1016/j.cageo.2018.03.001.

Passchier C.W. & Trouw R.A.J. (2005) - Microtectonics. Springer, Berlin, Heidelberg, pp. 366, https://doi.org/10.1007/3-540-29359-0.

Petroccia A., Bonasera M., Caso F., Nerone S., Morelli M., Bormioli D. & Moletta G. (2020) - Structural and geomorphological framework of the upper Maira Valley (Western Alps, Italy): the case study of the Gollone Landslide. Journal of Maps, 16(2), 534-542. https://doi.org/10.1080/17445647.2020.1784806.

Petroccia A., Montomoli C., Iaccarino S., & Carosi R. (2022) - Geology of the contact area between the Internal and External Nappe Zone of the Sardinian Variscan Belt (Italy): new insights on the complex polyphase deformation occurring in the hinterland-foreland transition zone of collisional belts. Journal of Maps, 1-12. https://doi.org/10.1080/17445647.2022.2093660.

Pesenti C., Zucali M., Manzotti P., Diella V. & Risplendente A. (2012) - Linking U-Th-Pb monazite dating to partial melting microstructures: Application to the Valpelline series (Austroalpine domain, Western Alps). Rendiconti Online Società Geologica Italiana, 22, 183-185.

Redler C., Johnson T.E., White R.W. & Kunz B.E. (2012) - Phase equilibrium constraints on a deep crustal metamorphic field gradient: metapelitic rocks from the Ivrea Zone (NW Italy). J. Metam. Geol., 30(3), 235-254, https://doi.org/10.1111/j.1525-1314.2011.00965.x.

Roda M., Zucali M., Corti L., Visalli R., Ortolano G. & Spalla M.I. (2021) - Blueschist mylonitic zones accommodating syn-subduction exhumation of deeply buried continental crust: The example of the Rocca Canavese Thrust Sheets Unit (Sesia-Lanzo Zone, Italian Western Alps). Swiss J. Geosci., 114, 6-39, https://doi.org/10.1186/s00015-021-00385-7.

Spalla M.I. & Zucali M. (2004) - Deformation vs. metamorphic re-equilibration heterogeneities in polymetamorphic rocks: a key to infer quality PTdt path. Rivista Italiana di Mineralogia e Petrologia, 73(249), 227-247.

Spalla M.I., Zucali M., Di Paola S. & Gosso, G. (2005) - A critical assessment of the tectono-thermal memory of rocks and definition of tectono-metamorphic units: evidence from fabric and degree of metamorphic transformations. Geological Society, London, Special Publications, 243(1), 227-247, https://doi.org/10.1144/GSL.SP.2005.243.01.16.

Sawyer, E.W. (2000) - Grain-scale and outcrop-scale distribution and movement of melt in a crystallising granite. Earth and Environmental Science Transactions of the Royal Society of Edinburgh, 91(1-2), 73-85, https://doi.org/10.1017/S0263593300007306.

Sawyer E.W. (2008) - Working with Migmatites. Short Course Series: Mineralogical Association of Canada, volume 38. Quebec: Mineralogical Association of Canada, 158 pp.

Tomkins H.S., Powell R. & Ellis D.J. (2007) - The pressure dependence of the zirconium–in–rutile thermometer. J. Metam. Geol., 25(6), 703-713, https://doi.org/10.1111/j.1525-1314.2007.00724.x.

Visalli R., Ortolano G., Godard G. & Cirrincione R. (2021) - Micro-Fabric Analyzer (MFA): A New Semiautomated ArcGIS-Based Edge Detector for Quantitative Microstructural Analysis of Rock Thin-Sections. ISPRS Int. J. Geo-Inf. 2021, 10, 51, https://doi.org/10.3390/ijgi10020051.

White R.W., Powell R., Holland T.J.B., Johnson T.E. & Green E.C.R. (2014) - New mineral activity–composition relations for thermodynamic calculations in metapelitic systems. J. Metam. Geol., 32, 261-286, https://doi.org/10.1111/jmg.12071.

Whitney D.L. & Evans B.W. (2010) - Abbreviation for names of rock-forming minerals. Am. Mineral., 95, 185-87, https://doi.org/10.2138/am.2010.3371.

Yakymchuk C. (2020) - Migmatites. In: Alderton D., Elias S.A. (Eds), Enciclopedia of Geology (Second edition), Academic press, 492-501, https://doi.org/10.1016/B978-0-08-102908-4.00021-7.

Zucali M., Manzotti P., Diella V., Pesenti C., Risplendente A., Darling J. & Engi M. (2011) - Permian tectonometamorphic evolution of the Dent-Blanche Unit (Austroalpine domain, Western Italian Alps). Rendiconti online Società Geologica Italiana, 15, 133-136.

Zucali M., Corti L., Roda M., Ortolano G., Visalli R. & Zanoni D. (2021) - Quantitative X-ray Maps Analysis of Composition and Microstructure of Permian High-Temperature Relicts in Acidic Rocks from the Sesia-Lanzo Zone Eclogitic Continental Crust, Western Alps. Minerals, 11, 1421, https://doi.org/10.3390/min11121421.